Arch. Metall. Mater. **68** (2023), 3, 921-932

DOI: https://doi.org/10.24425/amm.2023.145455

YAO HUANG[1], XIANGUO YAN[1*], RUIZE YUAN[1], ZHI CHEN[1],
LIANG TANG[1], AO SHEN[1], XUEMEI NIU[1]

RESEARCH ON REDUCING RESIDUAL STRESS IN MILLING OF ALUMINUM ALLOY

The machining residual stress produced in the cutting process of aluminum alloy parts can easily lead to a scrap of the processed parts. In order to reduce the residual stress of aluminum alloy in the milling process, based on the Taguchi-Grey relational approach, the effects of different milling parameters on the residual stress and surface roughness of 2A12 aluminum alloy were studied. To reduce the residual stress and surface roughness of 2A12 aluminum alloy, optimized milling parameters were obtained. To further reduce the milling residual stress of 2A12 aluminum alloy, the samples processed by the optimized milling parameters were treated by cryogenic treatment and artificial aging. The residual stress of the sample was measured by the blind hole drilling method, and the evolution mechanism of the microstructure to reduce the machining residual stress was revealed. The results show that the combination of deep cooling treatment and oil bath aging can effectively reduce the residual stress on the machined surface of the aluminum alloy and facilitate a more uniform distribution of the residual stress inside the specimen. The effect of the coarse second phase on the residual stress in the microstructure is not significant, and the fine and diffusely distributed precipitation phase is beneficial to the reduction of the residual stress in the aluminum alloy.

Keywords: Taguchi-grey relational approach; Aluminum alloy milling process; Cryogenic treatment; Machining residual stress

1. Introduction

Al-Cu-Mg alloys have been widely used in the manufacture of aircraft structural parts due to their high specific strength, high hardness and good corrosion resistance [1]. However, in the process of machining aircraft monolithic components, the workpiece deformation is caused by the uneven initial stress distribution of the blank, asymmetric structure and imperfect processing technology, which makes the workpiece difficult to meet the design requirement [2]. The residual stress after heat treatment and machining is the main factor affecting dimensional stability. The residual stress of aircraft structural parts after machining is the stress that exists in the structural parts and keeps balance with the surroundings. During the cutting process of structural parts, the coupling effect of plastic deformation and the thermal effect of temperature gradient will produce machining residual stress, which will easily lead to the deformation of parts, affect the dimensional stability of aircraft structural parts, and lead to a scrap of machined parts.

The material and cutting parameters of structural parts will have a certain impact on the residual stress and surface roughness. Aircraft monolithic components have strict size and surface roughness requirements, so it is necessary to optimize the cutting parameters. Tarng et al. [3] found that the surface finish could be improved by 250% using optimized machining parameters. It is found that the residual stress is common in the machined parts, and it shows a certain law. Low cutting speed is conducive to the generation of residual compressive stress, and the feed rate will increase the depth of surface residual stress [4]. Low cutting speed is beneficial to the generation of residual compressive stress, and the depth of surface residual stress will be increased by feed rate [4]. Tang et al. [5] obtained the law of the effect of different milling parameters on the residual stress of the machined surface. During the cutting process, the machining parameters have a great influence on the quality of the machined part. The Taguchi method is an experimental method for optimizing individual response characteristics with as few trials as possible, providing a more systematic research framework for the experimental design of many process parameters [6-8]. Studying the dual response characteristic optimization of residual stress and surface roughness is more complex than the single response characteristic optimization. Gray correlation

[1] TAIYUAN UNIVERSITY OF SCIENCE AND TECHNOLOGY, SCHOOL OF MECHANICAL ENGINEERING, CHINA

* Corresponding author: yan_xg2008@126.com

analysis can effectively correlate the complex relationships between multiple response characteristics. Taguchi method is combined with gray correlation analysis to optimize the milling process parameters with the response characteristics of residual stress and surface roughness of the specimen surface.

In industrial production, the size of the part after cutting and machining to meet the requirements of use, however, the parts are seriously deformed after standing for several days, which can not meet the requirements of use. The reason is that the residual stress values remain high after the part has been machined, which leads to the deformation of the part. Therefore, other methods are needed to further reduce the residual stress in the machined parts. The common methods used to eliminate residual stresses in quenched aluminum alloys are mechanical methods and heat treatment [9-10]. However, the mechanical method is only applicable to eliminate residual stresses in parts with symmetry and simple structure. High temperatures and long holding times during heat treatment may affect the properties of the aluminum alloy. Therefore, the common methods used to eliminate residual stresses in quenched aluminum alloys no longer meet the needs of industrial applications. Cryogenic treatment is a method of non-destructive material modification and material strengthening at low temperatures using liquid nitrogen as refrigerant, which is a technology in line with the green manufacturing category and is a continuation of the heat treatment process [11-12]. Cryogenic treatment improves the serviceability of the part by optimizing the microstructure. Several studies have confirmed that the combination of cryogenic treatment and artificial aging can reduce the residual stresses in aluminum alloys after quenching. For example, Araghchi M. [13] used a combination of cryogenic treatment and artificial aging to reduce the residual stress of the aluminum alloy by 71%. Weng et al. [14] demonstrated that the combination of cryogenic treatment and conventional heat treatment effectively reduced the residual stresses in aluminum alloy after quenching and improved the dimensional stability of aluminum alloy parts. Wang [15] proposed a deep-cooling process called “counter-quenching”, in which aluminum alloy components are immersed in liquid nitrogen and then “counter-quenched” using an organic medium to eliminate the residual stresses after quenching of 7050 aluminum alloy. However, there are few studies on the reduction of machined residual stresses in aluminum alloys using a combination of cryogenic treatment and artificial aging.

Based on this, the present work is devoted to the study of the process to reduce the residual stress in the milling of aluminum alloy. The Gray-Taguchi method was used to study the effect of different milling process parameters on the residual stresses and surface roughness of specimens milled from 2A12 aluminum alloy. The optimized milling process parameters were obtained with the objective of reducing residual stresses and surface roughness in the milling of 2A12 aluminum alloy. To further reduce the residual stresses in the milling of 2A12 aluminum alloy, the specimens processed by the optimized milling process parameters were subjected to deep cooling and artificial aging, and the residual stresses in the milling of 2A12 aluminum alloy before and after the deep cooling and artificial aging were analyzed by the blind hole method. To guide industrial applications, the evolutionary mechanism of the microstructure of the reduced machined residual stresses is revealed.

2. Experiments and methods

2.1. Milling test

The object of this work was the rolled 2A12 aluminum alloy. The chemical compositions of the 2A12 aluminum alloy were shown in TABLE 1. The milling test was carried out on a CM650 CNC milling machine with the specimen size of 100 mm × 100 mm × 20 mm, the tool is a four-tooth carbide end mill produced by Zhejiang Zhonghong CNC Tools Company, Ltd., and the parameters of the tool were $\phi 12 \times 30 \times 75$, helix angle 30°, front angle 15°, back angle 14°, and blunt radius of the cutting edge was 0.02 mm.

TABLE 1

Chemical compositions of 2A12 aluminum alloy (wt%)

Cu	Mg	Mn	Fe	Zn	Si	Cr	Ni	Al
4.9	1.42	0.650	0.176	0.112	0.044	0.01	0.01	bal

In the milling process, according to the machining process manual, the feed per tooth was selected as a fixed value f_z = 0.05 mm. The spindle speed, milling depth, milling width and tool path have a great influence on the residual stress on the machined surface of aluminum alloy. In the Taguchi method, these process parameters were set as four factors, and the residual stress and roughness of the machined surface were used as evaluation indicators. The levels selected for each control factor in this study were shown in TABLE 2. Details of four-factors and three-levels orthogonal tests were shown in TABLE 3. The geometric model of the milling process and the different tool paths were shown in Fig. 1. Where the tool path consists of parallel unidirectional linear movements, the machining path always starts from a point on the same horizontal line and the tool moves in only one direction.

TABLE 2

Parameters levels definition

Level	Spindle speed (r/min) (A)	Milling depth (mm) (B)	Milling width (mm) (C)	Tool path (D)
1	2000	1	6	Single-way milling
2	4000	1.5	8	Reciprocating Milling
3	6000	2	10	S-shaped milling

TABLE 3

Description of the parameters of each test

Sample name	Spindle speed (r/min)	Milling depth (mm)	Milling width (mm)	Tool path
1	2000	1	6	Single-way milling
2	2000	1.5	8	Reciprocating Milling
3	2000	2	10	S-shaped milling
4	4000	1	8	S-shaped milling
5	4000	1.5	10	Single-way milling
6	4000	2	6	Reciprocating Milling
7	6000	1	10	Reciprocating Milling
8	6000	1.5	6	S-shaped milling
9	6000	2	8	Single-way milling

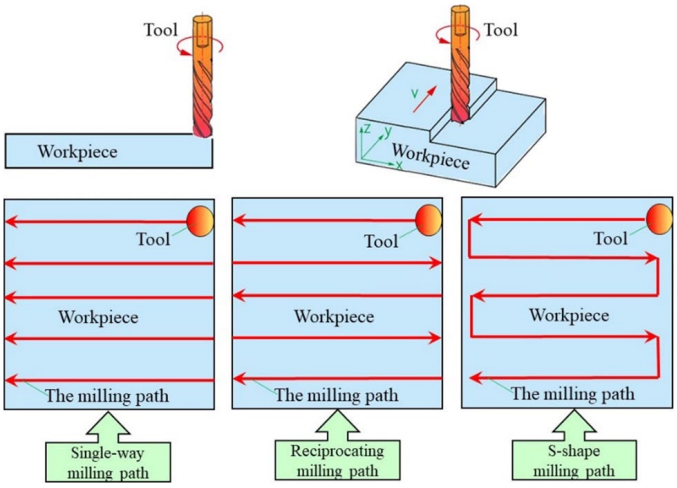

Fig. 1. Milling model and milling path diagram

2.2. Reduction of residual stress in machined parts by cryogenic treatment

Residual stress was commonly present in parts after cutting and machining, which can easily lead to cracks and fatigue damage. The combination of cryogenic treatment and conventional heat treatment can effectively reduce the residual stress in aluminum alloy [14]. Therefore, a combination of cryogenic treatment and artificial aging was used to reduce the residual stress of the machined parts. The optimized group of specimens with the least residual stress and surface roughness on the machined specimen surface is subjected to cryogenic treatment. The optimized cryogenic treatment process parameters of literature 16 were used to carry out the cryogenic treatment test by the program-controlled SLX-80 cryogenic system. The milled specimens were cooled to –196°C with a cooling rate of 3°C min^{-1} and held for 2 h before returning to room temperature. After that, the specimens were removed and placed in an oil bath at 180°C for 9 h for artificial aging [16]. The specific process parameters of the method combining cryogenic treatment with artificial aging were shown in TABLE 4.

TABLE 4

Process parameters for the combination of cryogenic treatment and artificial ageing

Specimen name	Cryogenic temperature/K	Cryogenic cycles	Holding time/h	Oil bath ageing
0	—	—	—	—
CT-1	–196°C	1	2h	Unoiled bath aging
CT-2	–196°C	1	2h	Oil bath aging 9 h
CT-3	–196°C	2	2h	Oil bath aging 9 h

2.3. Surface residual stress and surface roughness measurement

According to ASTM E837-2013, the residual stresses of the specimens were measured by the blind hole drilling method, as shown in Fig. 2. Fig. 2(a) shows the strain gauge sensitive grid arrangement by the blind hole method. As shown in Fig. 2(b), the BE120-2CD strain gauge rosette was attached to the samples as stated by the procedure provided by China Aviation Industry Electro-Mechanical Instrument Group Ltd. The RS-200 drilling unit was used to drill blind holes with a diameter of 1.803 mm and

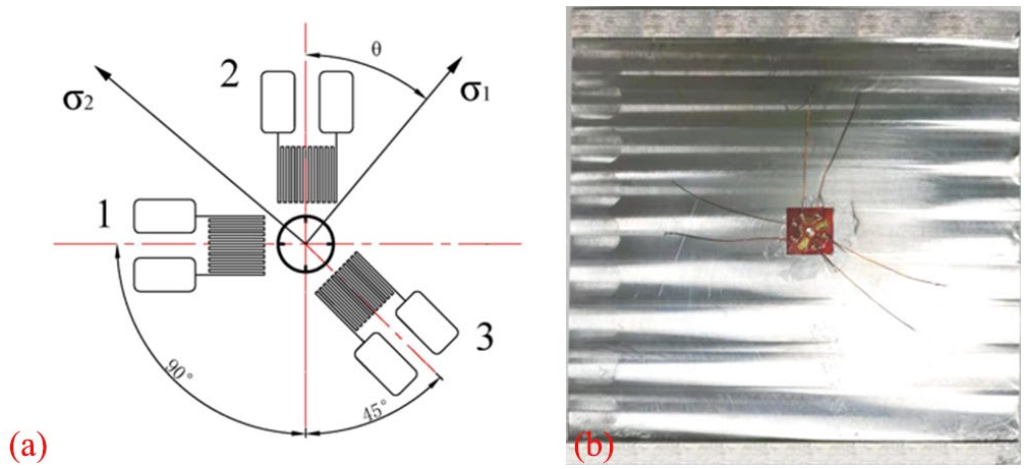

Fig. 2. Residual stress gauge (a) Strain gauge sensitive grid diagram (b) BE120-2CD

a depth of 2 mm in the specimen by means of an end mill driven by a high-speed air turbine with a speed of 20,000-400,000 rpm. After recording the strain values using the D4 model data collector, the non-uniform stresses were calculated based on the integral method by the borehole residual stress calculation program software [14]. All test points were at the same location of the specimen.

The surface roughness is the average arithmetic deviation of the absolute value of the distance from the top point to the center-line of the surface profile of the specimen, measured using the WALE- SP1103M-sgk-Y profilometer to measure the surface profile of the specimen and calculate the surface roughness of the specimen by Eq. (1).

$$Ra \approx \frac{1}{n}\sum_{i=1}^{n}|y| \tag{1}$$

Where Ra is the surface roughness of the specimen, n is the number of surface profile test points, and $|y|$ is the absolute value of the distance from each point on the surface profile to the center line.

2.4. Microstructure analysis

In order to study the changes in microstructure, the specimens were ground by 400, 800, 1200, 2000 and 3000 grit sandpaper and then mechanically polished, and the main component of the abrasive on the sandpaper was silicon carbide. Dip a cotton swab into a mixture of 3% hydrofluoric acid, 6% nitric acid, 91% water and wipe the surface of the specimen after mechanical polishing repeatedly for 5 seconds, rinse with plenty of alcohol and then dry the surface of the specimen quickly with a hair-dryer. Optical microscopy and electron scanning microscopy were used to observe the microstructure.

3. Results and discussion

3.1. Gray correlation analysis

In order to carry out multi-objective data optimization processing efficiently and scientifically, Gray Taguchi analysis was performed on the TABLE 5 orthogonal test data, which was divided into the following four steps, as shown in Fig. 3.

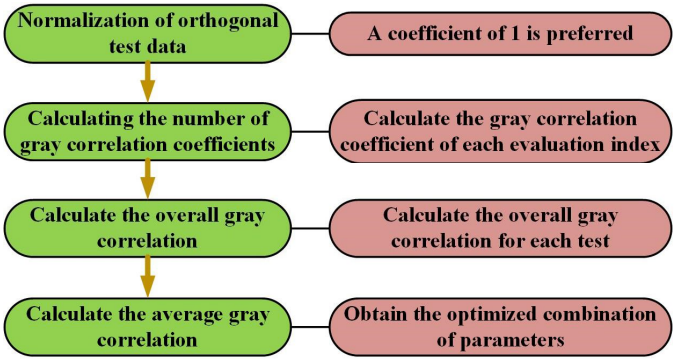

Fig. 3. Gray Taguchi analysis steps

3.1.1. Performance metrics data normalization process

According to the orthogonal array of the Taguchi method, a machining test was carried out on the 2A12 aluminum alloy workpiece, and the test results were shown in TABLE 5. The symbol of residual stress indicates the direction of residual stress. As can be seen from TABLE 5, the residual stresses on the machined specimen surfaces are all compressive stresses. In order to improve the comparability of the test data of each performance index, the test indexes were converted to standardized dimensionless values. The improvement of aluminum alloy milling performance is based on the reduction of surface residual stress and surface roughness, so the test data of surface residual stress and surface roughness are normalized with the goal of minimizing surface residual stress and surface roughness. The test data were normalized according to Eq. (2), and the results of the normalized test data are shown in TABLE 6.

$$Z_{ij} = \left(\max(x_{ij}) - x_{ij}\right)/\left(\max(x_{ij}) - \min(x_{ij})\right) \tag{2}$$

where Z_{ij} is the normalized value of the i trial of the j evaluation index, x_{ij} is the data of the i trial of the j evaluation index, $\max(x_{ij})$ is the maximum data among all trials in the j^{th} evaluation

TABLE 5

Experimental results for the machining trials conducted

Sample name	Spindle speed (r/min)	Milling depth (mm)	Milling width (mm)	Tool path	Residual stress (MPa)	Surface roughness (μm)
1	2000	1	6	Single-way milling	–59	0.296
2	2000	1.5	8	Reciprocating Milling	–36	0.995
3	2000	2	10	S-shaped milling	–70	0.806
4	4000	1	8	S-shaped milling	–32	1.289
5	4000	1.5	10	Single-way milling	–25	0.923
6	4000	2	6	Reciprocating Milling	–16	0.315
7	6000	1	10	Reciprocating Milling	–23	1.146
8	6000	1.5	6	S-shaped milling	–28	1.052
9	6000	2	8	Single-way milling	–25	1.04

TABLE 6

Results of normalization of experimental data

Sample name	Spindle speed (r/min)	Milling depth (mm)	Milling width (mm)	Tool path	Residual stress	Surface roughness
1	2000	1	6	Single-way milling	0.2037	1.0000
2	2000	1.5	8	Reciprocating Milling	0.6296	0.2961
3	2000	2	10	S-shaped milling	0.0000	0.4864
4	4000	1	8	S-shaped milling	0.7037	0.0000
5	4000	1.5	10	Single-way milling	0.8333	0.3686
6	4000	2	6	Reciprocating Milling	1.0000	0.9809
7	6000	1	10	Reciprocating Milling	0.8704	0.1440
8	6000	1.5	6	S-shaped milling	0.7778	0.2387
9	6000	2	8	Single-way milling	0.8333	0.2508

index, and $\min(x_{ij})$ is the minimum data among all trials in the j evaluation index [17]. Residual stress and surface roughness are the 2 evaluation indicators in the test. Therefore, the number of tests $i \leq 9$, the evaluation index $j \leq 9$.

The milling performance index is normalized according to the principle of "the smaller the better", and the larger the normalized value, the better the milling performance index. Therefore, a normalized value of 1 indicates the best results of the test [18]. The test data were normalized to be uniformly distributed, laying the foundation for gray correlation analysis of the data.

3.1.2. Calculating gray correlation coefficients

The gray correlation coefficient, as a coefficient to evaluate the potential of each parameter to establish correlation with performance indicators, can describe the degree of association between the original series of data and comparable series, also known as the degree of correlation [19]. Where, the closer the gray correlation coefficient value of the target output is to 1, the better the correlation is, and the gray correlation coefficient is obtained from Eq. (3). Where, Δ_{ij} is the mass loss function $\Delta_{ij} = |\overline{y_{ij}} - y_{ij}|$, $\overline{y_{ij}}$ is the target value after standardizing the test data of the i^{th} evaluation index, $\overline{y_{ij}} = 1$; $\Delta_{\min} = \min_i \min_j \Delta_{ij}$, $\Delta_{\max} = \max_i \max_j \Delta_{ij}$, δ is the resolution factor, $\delta = 0.5$ [17]. The calculation results are shown in TABLE 7. As can be seen from TABLE 7, the gray correlation coefficient between the residual stress of the 6th orthogonal test and the surface roughness of the 1st orthogonal test is the largest, indicating the best correlation of their parameter combinations.

$$\xi_{ij} = \left(\Delta_{\min} + (\delta * \Delta_{\max})\right) / \left(\Delta_{ij} + (\delta * \Delta_{\max})\right) \tag{3}$$

3.1.3. Calculating the overall gray correlation

To further evaluate the strengths and weaknesses of each group of experimental data, the concept of overall gray correlation was introduced for comprehensive evaluation. The overall gray correlation degree evaluates all performance index values can be used as the basis for determining the orthogonal test group, and the larger its overall gray correlation degree value, the better the test results synthesized for the corresponding parameter level [20]. The overall gray correlation coefficient was obtained from Eq. (4).

$$\beta_i = (1/n) / \sum_{j=1}^{n} \xi_{ij} \tag{4}$$

Where β_i is the grey relational grade for i^{th} response, n is the total number of grey relational coefficients and ξ_{ij} is the grey

TABLE 7

Results of normalization of experimental data

Sample name	Processing parameters				Grey relational coefficient		Overall gray correlation	Rank
	Spindle speed (r/min) A	Milling depth (mm) B	Milling width (mm) C	Tool path D	Residual stress	Surface roughness		
1	2000	1	6	Single-way milling	0.3857	1.0000	0.6929	2
2	2000	1.5	8	Reciprocating Milling	0.5745	0.4153	0.4949	7
3	2000	2	10	S-shaped milling	0.3333	0.4933	0.4133	9
4	4000	1	8	S-shaped milling	0.6279	0.3333	0.4806	8
5	4000	1.5	10	Single-way milling	0.7500	0.4419	0.5960	3
6	4000	2	6	Reciprocating Milling	1.0000	0.9631	0.9816	1
7	6000	1	10	Reciprocating Milling	0.7941	0.3687	0.5814	4
8	6000	1.5	6	S-shaped milling	0.6923	0.3964	0.5444	6
9	6000	2	8	Single-way milling	0.7500	0.4002	0.5751	5

relational coefficient for i^{th} trial for j^{th} independent response. As can be seen from TABLE 7, the overall gray correlation of the group 6 orthogonal test is 0.9816, which has the highest overall gray correlation value. Therefore, the 6th group of orthogonal tests is the best combination of process parameters as follows: reciprocal milling path, 4000 rpm spindle speed, 2 mm milling depth and 6 mm milling width.

3.1.4. Calculating the average gray correlation

According to the principle of orthogonal test design, the best combination of milling processing parameters may be distributed outside of the nine sets of test combinations. Therefore, further data analysis of the gray correlation values for each group of tests is required to obtain the optimal combination of processing parameters. The average gray correlation can visualize the correlation between the level of each factor and the performance evaluation index. The maximum average gray correlation of each factor indicates that its corresponding factor level has the greatest influence on the performance evaluation index. To further determine the optimal combination of machining parameters for aluminum alloy milling, the average gray correlation of each factor level was calculated based on the overall gray correlation values of nine sets of orthogonal tests, and the calculated results are shown in TABLE 8. To easily observe the average gray correlation response at each factor level, an average gray correlation graph was created, as shown in Fig. 4, the different states of each factor in the orthogonal test are called levels. There are four factors in the milling process (spindle speed, milling depth, milling width and tool path), and three different levels are set for each factor, and the specific level values of each factor are shown in TABLE 2.

TABLE 8

Average gray correlation table

Level	Processing parameters (Factors)			
	Spindle speed (A)	Milling depth (B)	Milling width (C)	Tool path (D)
1	0.5337	0.5850	0.7396	0.6213
2	0.6861	0.5451	0.5169	0.6860
3	0.5670	0.6567	0.5302	0.4794
Extreme differences	0.1524	0.1116	0.2227	0.2065
Rank	3	4	1	2

From TABLE 8 and Fig. 4, it can be seen that the average gray correlation of the 2nd level of spindle speed (A) (4000 rpm), the 3rd level of milling depth (B) (2 mm), the 1st level of milling width (C) (6 mm) and the 2nd level of tool path (D) (Reciprocating Milling) is the highest, so the best combination of machining parameters for milling aluminum alloy is $A_2B_3C_1D_2$, which are Reciprocating milling as tool path strategy, 4000 rpm spindle speed, 2 mm milling depth and 6mm milling width. In order to determine the primary and secondary relationships of the influence of each machining parameter on the milling performance of aluminum alloy, the mean gray correlation of each factor was subjected to extreme difference analysis. The results of the extreme difference analysis in TABLE 8 show the degree of influence of each milling process parameter on the milling performance. Milling width has the greatest impact on milling performance, followed by tool milling path, then spindle speed, with the least impact on milling depth. As can be seen from Fig. 4, the residual stress and surface roughness on the machined specimen surface tends to increase and then decrease with the increase of spindle speed during the milling process of aluminum alloy, the residual stress and surface roughness on the machined specimen surface tend to decrease and then increase with the increase of milling depth, the residual stress and surface roughness on the machined specimen surface tend to decrease and then increase with the increase of milling width, and the residual stress and surface roughness on the machined specimen surface tend to decrease and then increase with the increase of milling width. The residual stresses and surface roughness of the machined specimen surface tend to decrease and then increase with the increase of milling width, and the residual stresses and surface roughness of the machined specimen surface are the smallest when the reciprocating milling path was used for milling.

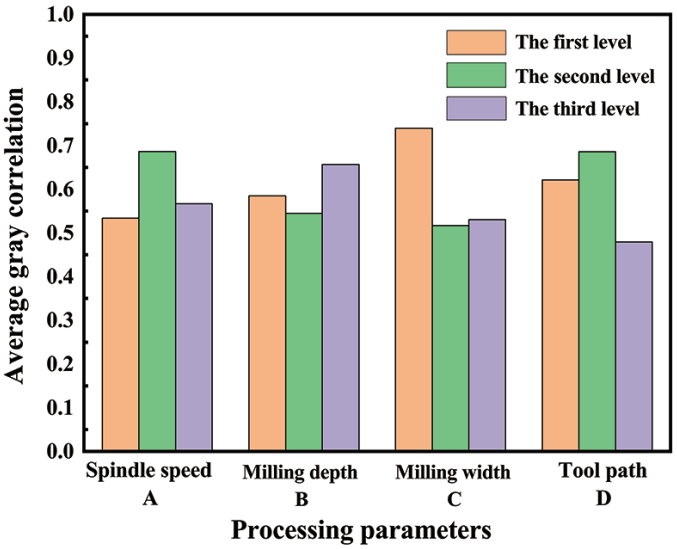

Fig. 4. Average gray correlation chart

3.2. Analysis of variance

From the above analysis, it is clear that the milling depth has the lowest contribution to the milling performance, so analysis of variance (ANOVA) was performed on the other three factors to determine the contribution of each factor to the milling performance. The overall gray correlation data for each combination of factor levels in the processing parameters were analyzed by analysis of variance (ANOVA) using Minitab 19 software (Shanghai Tecma Information Technology Ltd.), and the results are shown in TABLE 9. As can be seen from TABLE 9,

among the three factors, milling width (Factor C) has the largest contribution of 42.9%, tool path (Factor D) has the second- largest contribution of 30.7%, and spindle speed (Factor A) has the smallest contribution of 17.6%. From the above analysis, it can be seen that the two factors of milling width and tool path contribute significantly to the residual stress and surface roughness of the machined specimen surface, so the interaction of milling width and tool path on the residual stress and surface roughness of the machined specimen surface was analyzed, as shown in Fig. 5. The overall gray correlation variance interaction plot shows that there is some interaction between the two factors of milling width and tool path.

TABLE 9

Overall gray correlation analysis of variance

Factors	Degree of freedom	Sum of squares	Sum of mean squares	F value	Contribution rate (%)
Spindle speed (Factor A)	2	0.03850	0.019252	2.01	17.6
Milling width (Factor C)	2	0.09361	0.046807	4.88	42.9
Tool path (Factor D)	2	0.06697	0.033483	3.49	30.7
Error	2	0.01919	0.009594		8.8
Total	8	0.21827			100

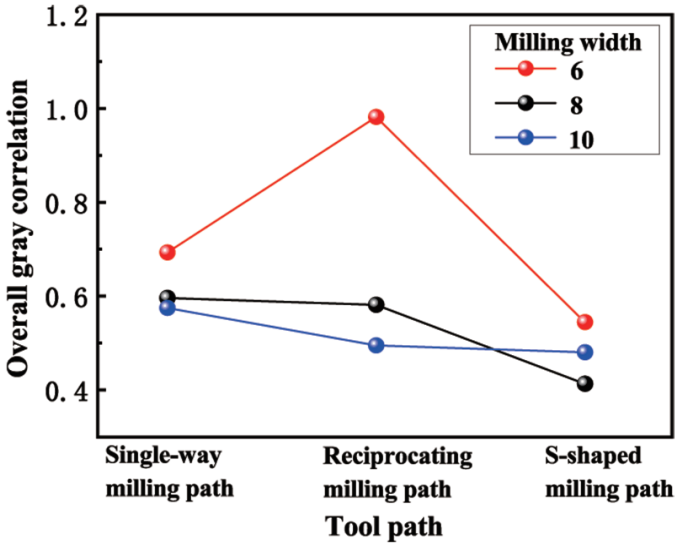

Fig. 5. Overall gray correlation variance interaction diagram

3.3. Analysis of the results of the combination of cryogenic treatment and artificial aging for the reduction of residual stresses in machined specimens

The results of the optimized group of specimens with the least residual stress and surface roughness on the machined specimen surface after different cryogenic treatment processes are shown in Fig. 6. From the above analysis, it can be seen that the residual stress on the surface of specimen 0 after machining with the optimized milling process parameters (Reciprocating milling as tool path strategy, 4000 rpm spindle speed, 2 mm milling depth and 6mm milling width) by Gray Taguchi is 16 MPa. The residual stress on the surface of the machined specimen CT-1 (cryogenic temperature –196°C, cryogenic times 1 time, holding time 2 h, no oil bath aging treatment process) is 15 MPa, which is similar to the residual stress value on the surface of the machined specimen 0 without cryogenic treatment. The residual stress on the surface of the specimen CT-2 (cryogenic temperature –196°C, cryogenic times 1 time, holding time 2 h, oil bath aging 9 hours treatment process) was 11 MPa, which was slightly lower than the residual stress on the surface of the processed specimens treated with the specimen CT-1 (cryogenic temperature –196°C, cryogenic times 1 time, holding time 2 h, no oil bath aging treatment process). The specimen CT-1 and the specimen CT-2 (cryogenic temperature –196°C, cryogenic times 1 time, holding time 2 h, oil bath aging 9 hours treatment process) have the same cryogenic treatment process, the difference is that the specimen CT-2 adds oil bath aging after the end of the cryogenic treatment. It shows that the oil bath aging has an effect on the surface residual stress of the machined aluminum alloy specimens. The residual stress on the surface of the specimen CT-3 (cryogenic temperature –196°C, cryogenic times 2 time, holding time 2 h, oil bath aging 9 hours treatment process) was 3 MPa, and the residual stress on the surface of machined specimens treated with this group of processes was the smallest. The specimen CT-2 and the specimen CT-3 in the oil bath aging process are the same, the difference is that the specimen CT-3 in the first cryogenic treatment and oil bath aging between another cryogenic treatment. It shows that the number of cryogenic treatment has a significant effect on the residual stress on the surface of machined aluminum alloy specimens.

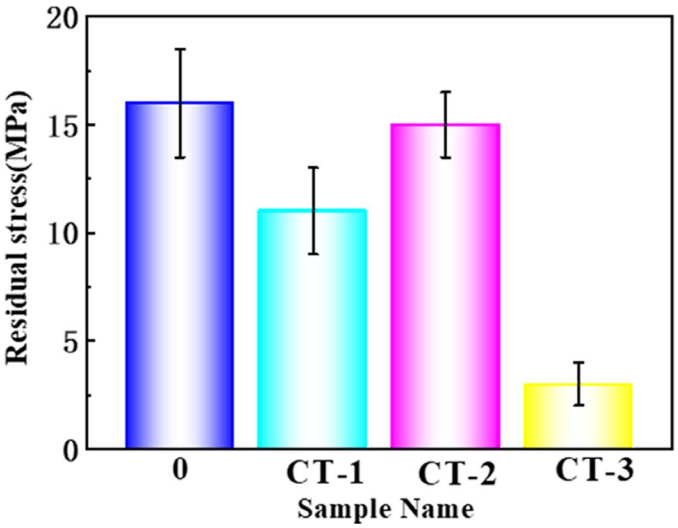

Fig. 6. Residual stress on the surface of specimens after different cryogenic treatment processes

In order to further analyze the residual stresses of the machined specimens, the blind hole method was used to measure the residual stresses at different depths of the machined aluminum

alloy specimens. The location of the residual stress test point of the machined aluminum alloy specimen is shown in Fig. 7. The measurement depth of the blind hole method for this test is 0.4 mm, and the results of the residual stress measurement by the blind hole method are shown in Fig. 8. As can be seen from Fig. 8, the residual stress of machined aluminum alloy specimen 0 without cryogenic treatment fluctuates in the depth direction, and with the increase of depth, the residual stress of machined aluminum alloy specimen 0 shows tensile stress first and then compressive stress. This is due to the large internal stresses in the quenched specimens [21] and the uneven distribution of internal stresses under the coupling effect of cutting forces and cutting heat during the cutting process leading to significant fluctuations in the internal residual stresses in the machined specimens. The residual compressive stress in the specimen CT-1 (cryogenic temperature –196°C, cryogenic times 1 time, holding time 2 h, no oil bath aging) increases with increasing depth. The residual stresses in the specimen CT-2 (cryogenic temperature –196°C, cryogenic times 1 time, holding time 2 h, oil bath aging 9 hours) decrease with increasing depth and the residual tensile stresses inside the specimens decrease and the residual compressive stresses increase, tending to compressive stresses inside the specimens. As can be seen from the curves in Fig. 8, the residual stress values of the specimen CT-3 (cryogenic temperature –196°C, cryogenic times 2 time, holding time 2 h, oil bath aging 9 hours) remain around 0 MPa with increasing depth, and hardly change with increasing depth. The residual stresses in the specimen CT-2 (cryogenic temperature –196°C, cryogenic times 1 time, holding time 2 h, oil bath aging 9 hours) and the specimen CT-3 (cryogenic temperature –196°C, cryogenic times 2 time, holding time 2 h, oil bath aging 9 hours) process fluctuated less, indicating that the oil bath aging facilitated a more uniform distribution of residual stresses within the specimens.

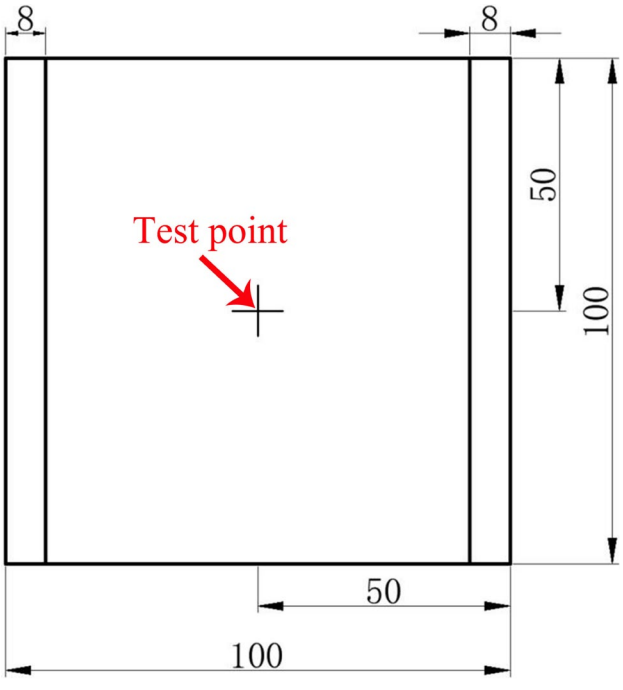

Fig. 7. Location of residual stress test points

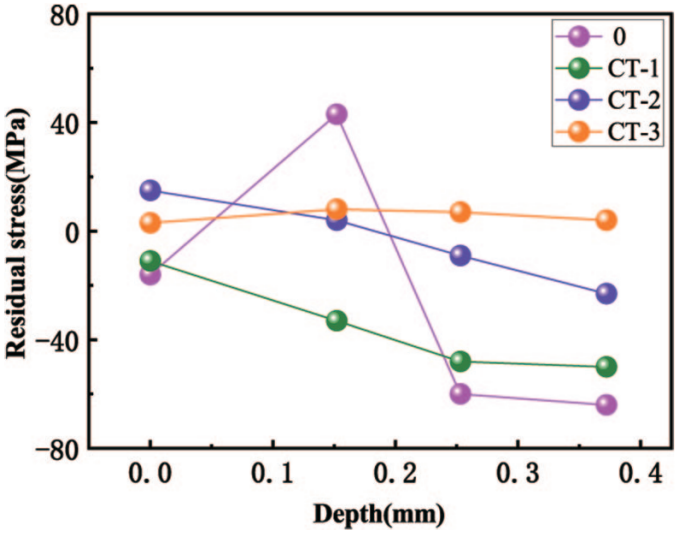

Fig. 8. Residual stresses at different depths

3.4. Microstructure analysis

In order to analyze the mechanism of the effect of cryogenic treatment and artificial aging on the residual stresses in the machined specimens, the microstructure of the aluminum alloy was observed. The microstructure of the machined specimens of 2A12 aluminum alloy was observed by optical microscopy, as shown in Fig. 9. The composition of the material phase in the microstructure was tested by X-ray diffraction method, as shown in Fig. 10. The size of the grains is determined by the truncation method for the metallographic picture of the specimen, which is calculated by Eq. (5).The size of the grains was determined by the truncation method for the metallographic diagram of the specimen, and the number of grains per unit area in the microstructure of the processed specimen 0 without cryogenic treatment was 12, and the number of grains per unit area in the microstructure of the specimen after cryogenic treatment was higher than 108, so the grains of the processed specimen with cryogenic treatment were finer than those of the processed specimen 0 without cryogenic treatment. From Fig. 9(a) and Fig. 10(a), it can be seen that the microstructure of the machined 2A12 aluminum alloy specimen consists of the matrix and a small amount of undissolved coarse second phase particles, where the coarse second phase is the T phase (Al_6CuMg_4). As can be seen from Fig. 9(a), the size of the coarse second phase T-phase (Al_6CuMg_4) in the microstructure of the machined specimen 0 without cryogenic treatment is 62.5 μm, which is mainly distributed near the grain boundaries. From Fig. 9(b), it can be seen that the size of the coarse second phase T-phase (Al_6CuMg_4) is 40.6 μm in the microstructure of the specimen CT-1 (cryogenic treatment Process parameters are cryogenic temperature –196°C, 1 time of deep cooling, holding time 2 h, no oil bath aging). From Fig. 9(c), it can be seen that the size of the coarse T-phase (Al_6CuMg_4) in the microstructure of the specimen CT-2 (cryogenic treatment Process parameters are cryogenic temperature –196°C, number of deep cooling

times 1, holding time 2 h, and oil bath aging 9 hours) is 43.8 μm. From Fig. 9(d), it can be seen that the size of the coarse T-phase (Al_6CuMg_4) in the microstructure of the specimen CT-3 (cryogenic treatment Process parameters are cryogenic temperature –196°C, 2 times of deep cooling, holding time 2 h, and 9 hours of oil bath aging) is 40.6 μm, so the size of the T-phase (black part in the figure) of the deep-cooled specimen is smaller than that of the machined specimen 0 without cryogenic treatment, and is diffusely and uniformly distributed inside the grain. The fine grains in the microstructure causes the stresses in the matrix to be dispersed over more grains during micro-plastic deformation, resulting in a more uniform distribution of micro-plastic deformation in the matrix [22]. Micro-plastic deformation in the microstructure will release local residual stresses, so grain refinement can effectively reduce residual stresses in aluminum alloys. Grain refinement leads to an increase in the number of grains per unit volume in the microstructure, micro-plastic deformation can occur in more grains and is more uniform, effectively reducing stress concentration. Due to the principle of thermal expansion and contraction, the lattice shrinks at low temperatures. The lattice contraction decreases the lattice parameters and thus the ability to dissolve solute atoms [23], which promotes the precipitation of solute atoms. The effect of the coarse second phase on the residual stress in the microstructure is not significant, and the fine and diffusely distributed precipitation phase are beneficial to the reduction of the residual stress in the aluminum alloy.

$$n = N^2/L^2 \tag{5}$$

Where n is the number of grains per unit area, N is the number of grains tested, and L is the length of the test line (mm).

The microstructure of the machined specimens of 2A12 aluminum alloy was observed by scanning electron microscopy, as shown in Fig. 11. From Fig. 10(a) and Fig. 11(a), it can be seen that the coarse insoluble T-phase (Al_6CuMg_4) is distributed in the microstructure of the aluminum alloy without cryogenic treatment. From Fig. 10(b) and Fig. 11(b), it can be seen that the coarse insoluble T-phase (Al_6CuMg_4) is partially dissolved in the aluminum base and a large number of fine Al_2CuMg phases are precipitated in the microstructure of the specimen CT-1 without oil bath aging, but the Al_2CuMg phases are not uniformly distributed in the aluminum base. Therefore, cryogenic treatment can promote the precipitation of the second phase. Solids physically have the property of thermal expansion and contraction, and when the temperature changes, the volume of the solid changes accordingly, resulting in internal stresses in the object. The increase in lattice internal stress at low temperature provides the driving force for the precipitation

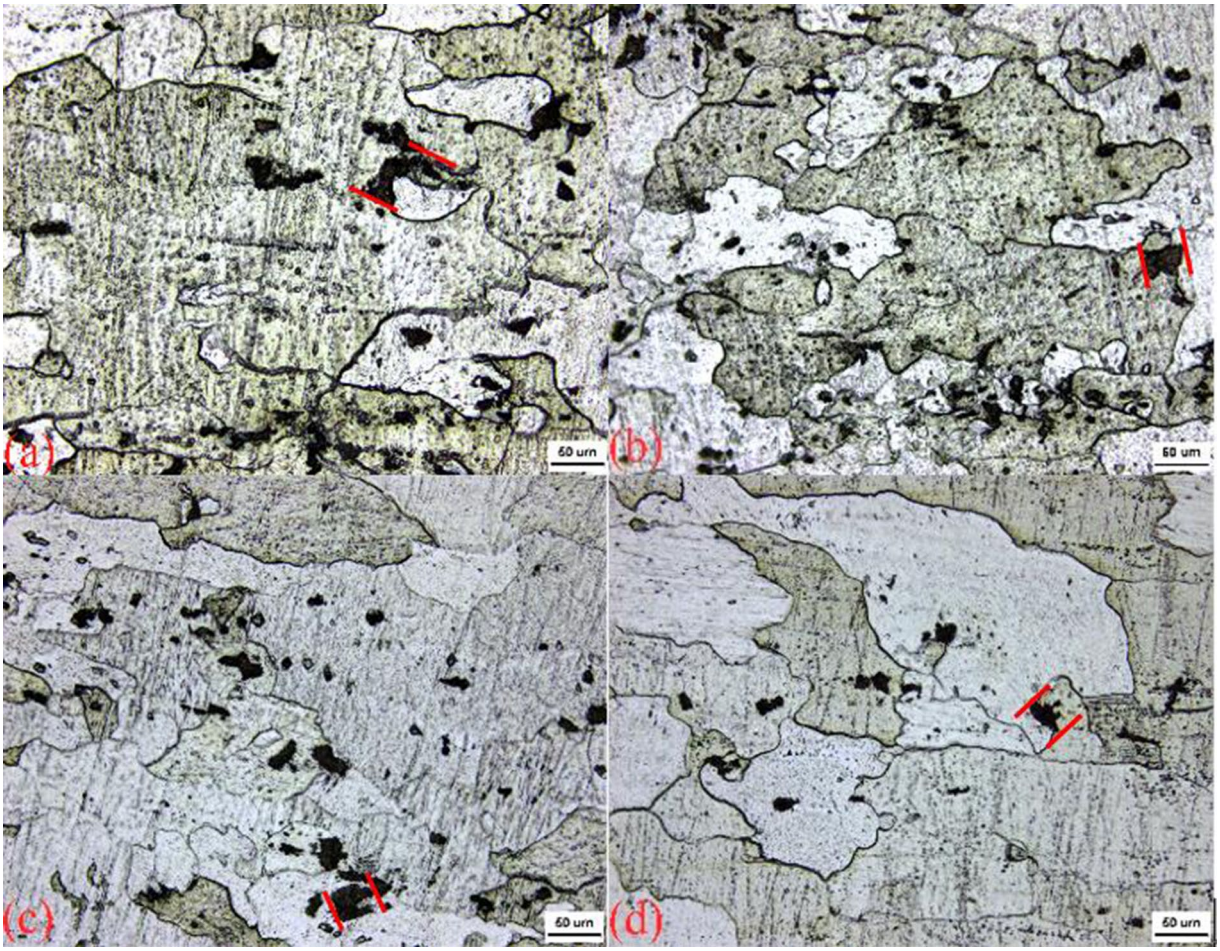

Fig. 9. Microstructure of the specimens treated by different processes under optical microscope: (a) Specimen 0 under optical microscope; (b) Specimen CT-1 under optical microscope; (c) Specimen CT-2 under optical microscope; (d) Specimen CT-3 under optical microscope

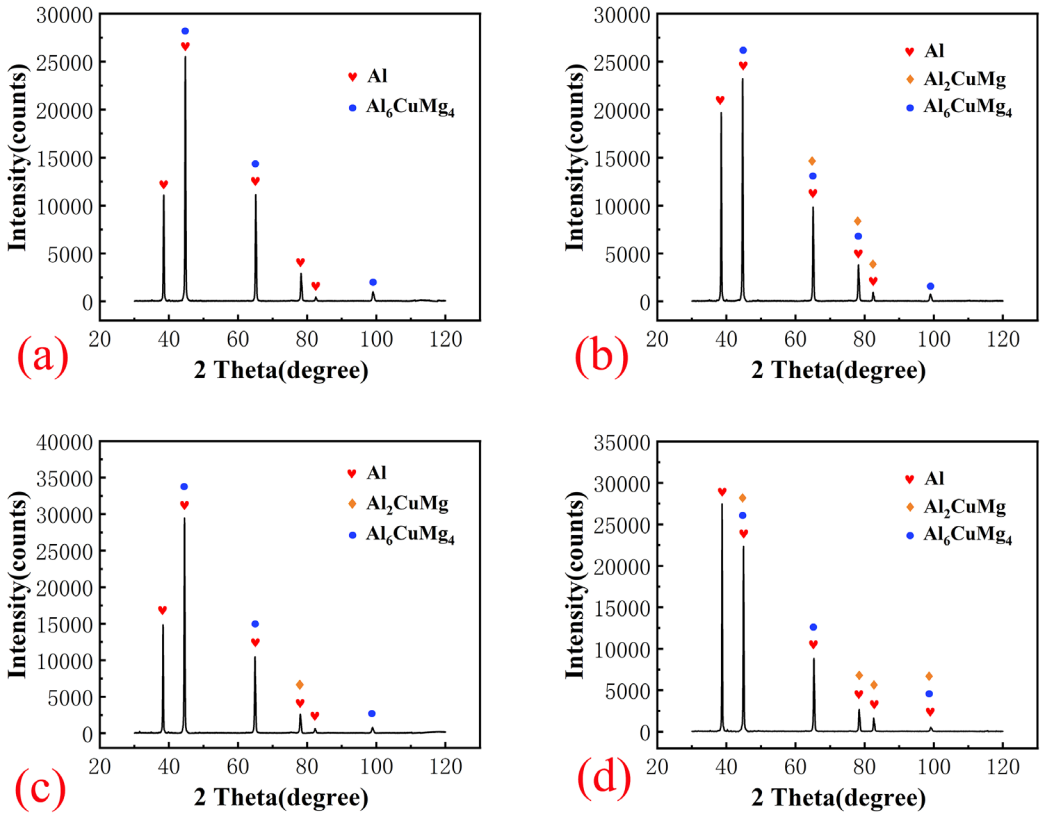

Fig. 10. X-ray diffraction pictures: (a) X-ray diffraction image of specimen 0; (b) X-ray diffraction picture of specimen CT-1; (c) X-ray diffraction images of specimen CT-2; (d) X-ray diffraction picture of sample CT-3

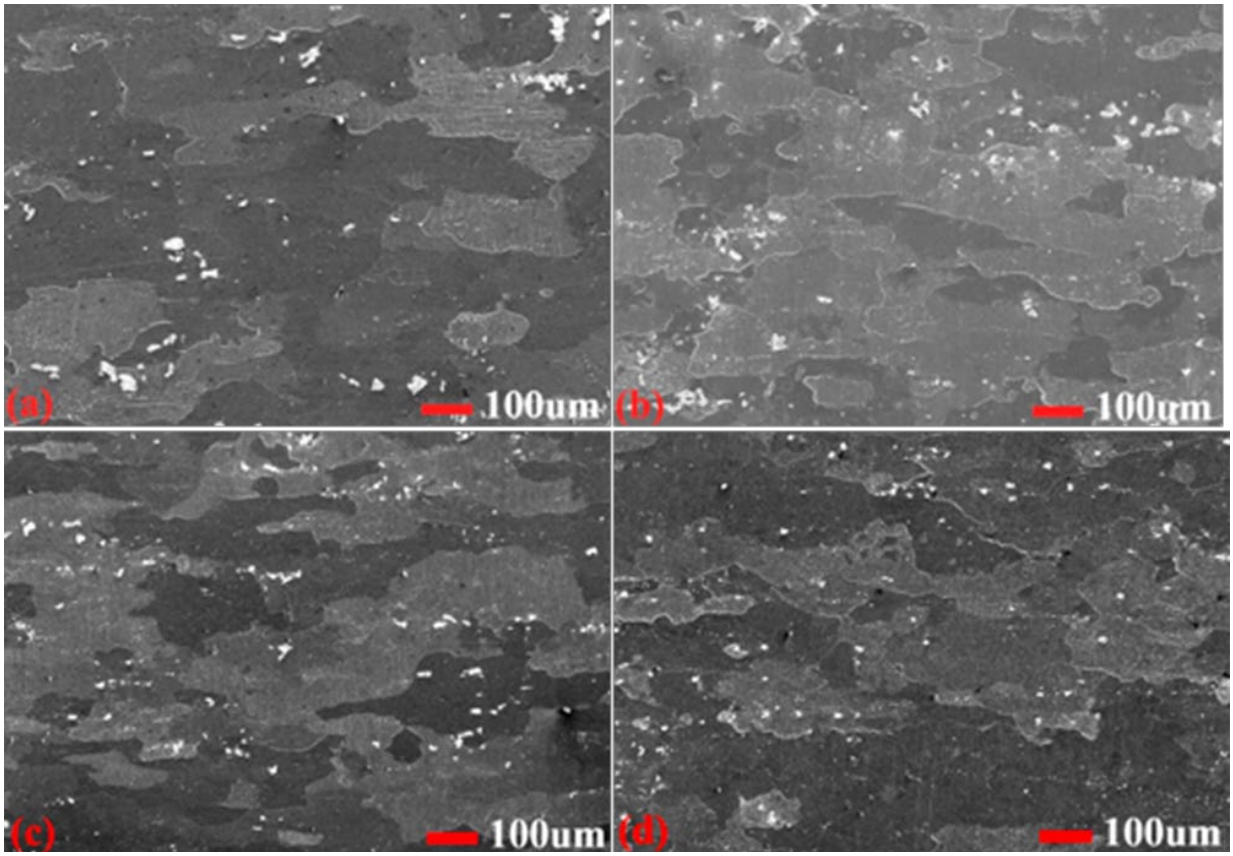

Fig. 11. Microstructure of the specimens treated by different processes under scanning electron microscope: (a) Specimen 0 under scanning electron microscope; (b) Specimen CT-1 under scanning electron microscope; (c) Specimen CT-2 under scanning electron microscope; (d) Specimen CT-3 under scanning electron microscope

of the second phase, so that a certain amount of fine second phase precipitates in the tissue after cryogenic treatment [16]. In order to determine the relationship between temperature and internal stress during cryogenic treatment, it is assumed that the volumes of the solids are V_0 and V_1, respectively, at temperatures from T_0 to T_1 in the isobaric process, and the volume shrinkage rate is $\phi = \Delta V/V$, i.e.:

$$\phi = \Delta V/V_0 = (V_1 - V_0)/V_0 = \\ = V_0[e^{\gamma(T_1-T_0)} - 1]/V_0 = e^{\gamma(T_1-T_0)} - 1 \quad (6)$$

in Eq. (6), $V_1 = V_0 e^{\gamma(T_1-T_0)}$, $\gamma = V^{-1}(\partial V/\partial T)P$, V is the volume and P is the pressure [24]. If the volume shrinkage is treated as volume strain, the average compressive stress $\overline{\sigma} = K\phi$ is obtained according to the volume Hooke's law, i.e.:

$$\overline{\sigma} = K\phi = K[e^{\gamma(T_1-T_0)} - 1] \quad (7)$$

in Eq. (7), $\overline{\sigma} = (\sigma_1 + \sigma_2 + \sigma_3)/3$, $K = E/[3(1 - 2\mu)]/3$, $\overline{\sigma}$ is the mean values of the three principal stresses, and K, E and μ are the bulk modulus of elasticity, the modulus of elasticity of the material and Poisson's ratio, respectively [24]. From Eq. (7), the relationship between temperature reduction and internal stresses during cryogenic treatment can be seen. The internal stress generated by the temperature reduction provides the driving force for the precipitation of the second phase. From Fig. 10(b), 10(c) and 10(d), it can be seen that the phases precipitated in the microstructure of the processed specimens after the cryogenic treatment are all Al_2CuMg phases. From Fig. 11 (b) and Fig. 11(c), it can be seen that the distribution of the precipitated phases in the microstructure of the cryogenic treatment specimen CT-2 aged in an oil bath is more uniform compared with that of the cryogenic treatment specimen CT-1 without oil bath aging. Aging treatment after cryogenic treatment can further promote the precipitation of phases [14]. Aging in an oil bath results in a more uniform distribution of the precipitated second phase (Al_2CuMg). From Fig. 11(c) and 11(d), it can be seen that the number of precipitated second phases (Al_2CuMg) in the microstructure of the cryogenic treatment specimen CT-3 aged in an oil bath is more and the size of the precipitated phases is finer and diffusely and uniformly distributed in the aluminum based compared with that of the cryogenic treatment specimen CT-2 aged in oil bath. The reason for this is that the specimen CT-3 underwent two cryogenic treatment processes prior to oil bath aging. The residual stresses in the alloy were reduced and uniformly distributed after the aluminum alloy was subjected to multiple cycles of cryogenic treatment [25]. The 2A12 aluminum alloy does not have smaller residual stress in the specimen the greater the number of deep cooling cycles, but rather the residual stress is minimized when the number of deep cooling cycles is two [16]. The structural stability of the tissue is significantly enhanced due to the cyclic multiple cryogenic treatments that divides the original grains into many sub-crystals, which interact and entangle with each other [26].

4. Conclusion

In this study, the effects of machining parameters (spindle speed, milling width, milling depth and tool path) on residual stress and surface roughness were investigated by Taguchi method, and the optimal combination of machining parameters with less residual stress and surface roughness was obtained based on the gray correlation analysis. A combination of cryogenic treatment and artificial aging is used to further reduce the residual stress on the machined aluminum alloy surface and to reveal the intrinsic micro-mechanisms. The main findings are shown below:

(1) In the aluminum alloy milling process, milling width has the most significant impact on milling performance, followed by tool milling path, then spindle speed, and the least impact on milling depth. The optimized combination of machining parameters obtained based on gray correlation analysis is: reciprocating milling path strategy, spindle speed 4000 rpm, milling depth 2 mm, and milling width 6 mm.

(2) The combination of cryogenic treatment and oil bath aging can effectively reduce the residual stress on the machined surface of the aluminum alloy and facilitate a more uniform distribution of the residual stress inside the specimen.

(3) The effect of the coarse second phase on the residual stress in the microstructure is not significant, and the fine and diffusely distributed precipitation phase were conducive to the reduction of residual stress in the aluminum alloy. The cryogenic treatment promotes the precipitation of the fine second phase in the aluminum alloy, and the oil bath aging further promotes the diffuse distribution of the fine second phase.

Acknowledgements

The authors gratefully acknowledge the support of Natural Science Foundation of Shanxi Province, China (202103021224280); Jincheng Science and Technology Plan Project, China (20198025); Excellent Graduate Innovation Project of Shanxi Province, China(2019SY476).

REFERENCES

[1] Y.B. Dong, W.Z. Shao, L.X. Lu, J. Mater. Eng. Perform. **24** (12), 4928-4940 (2015). DOI: https://doi.org/10.1007/s11665-015-1758-9

[2] X.Z. Wang, Z.L. Li, Q.Z. Bi, Int. J. Mach. Tools Manuf. **142**, 98-106 (2019). DOI: https://doi.org/10.1016/j.ijmachtools.2018.12.004

[3] W.P. Yang, Y. Tarng, J. Mater. Process. Technol. **84** (1-3), 122-129 (1998). DOI: https://doi.org/10.1016/S0924-0136(98)00079-X

[4] Q. Zhang, M. Mahfouf, J. Yates, Mater. Manuf. Process. **26** (3), 508-520 (2011). DOI: https://doi.org/10.1080/10426914.2010.537421

[5] Q. Tang, X. Zhao, D. Wang. Mod. mach. **01**, 1-4 (2016). DOI: https://doi.org/10.13667/j.cnki.52-1046/th.2016.01.001

[6] G. Taguchi, Introduction to quality engineering: designing quality into products and processes, McGraw-Hill, New York (1986).
[7] P.J. Ross, Taguchi techniques for quality engineering: loss function, orthogonal experiments, parameter and tolerance design, McGraw-Hill, New York (1988).
[8] J.R. Philip, Taguchi techniques for quality engineering, McGraw-Hill, New York (1988).
[9] G.H. Wu, J. Qiao, L.T. Jiang, Acta Metall. Sin. **55** (1), 33-44 (2019). DOI: https://doi.org/10.11900/0412.1961.2018.00482
[10] M. Koç, J. Culp, T. Altan, J. Mater. Process. Technol. **174**, 342-354 (2006). DOI: https://doi.org/10.1016/j.jmatprotec.2006.02.007
[11] M. Koneshlou, K.M. Asl, F. Khomamizadeh, Cryogenics. **51** (1), 55-61 (2011). DOI: https://doi.org/10.1016/j.cryogenics.2010.11.001
[12] A. Molinari, M. Pellizzari, S. Gialanella, J. Mater. Process. Technol. **118** (1-3), 350-355(2001). DOI: https://doi.org/10.1016/S0924-0136(01)00973-6S
[13] M. Araghchi, H. Mansouri, R. Vafaei, Mater. Sci. Eng. A. **689**, 48-52 (2017). DOI: https://doi.org/10.1016/j.msea.2017.01.095
[14] Z.J. Weng, X.Z. Liu, K.X. Gu, Mater. Sci. Technol. **36** (14), 1547-1555 (2020). DOI: https://doi.org/10.1080/02670836.2020.1800182
[15] Q.C. Wang, Research on residual stress relief and evaluation technology of aviation aluminum alloy, Thesis, Zhejiang University, Hangzhou, CN310058, October.
[16] X.M. Niu, Y. Huang, X.G. Yan, J. Mater. Eng. Perform. **30**, 1-10 (2021). DOI: https://doi.org/10.1007/s11665-021-06136-x
[17] J. Unnikrishnapillai, I. Sanghrajka, M. Shunmugavel, Measurement. **124**, 291-298 (2018). DOI: https://doi.org/10.1016/j.measurement.2018.04.052
[18] S.R. Zhao, Numerical simulation and parameter optimization of tap tapping process for machining 316L stainless steel, Thesis, Taiyuan University of Science and Technology, Taiyuan, CN 030024, June.
[19] G. Anand, N. Alagumurthi, R. Elansezhian, J. Braz. Soc. Mech. Sci. Eng. **40** (4), 214 (2018). DOI: https://doi.org/10.1007/s40430-018-1137-1
[20] H.S. Gau, C.Y. Hsieh, C.W. Liu, Stoch. Env. Res. Ris. A. **20** (6), 407-421(2006). DOI: https://doi.org/10.1007/s00477-006-0034-9
[21] R. Pan, T. Pirling, J.H. Zheng, J. Mater. Process. Technol. **264**, 454-468 (2019). DOI: https://doi.org/10.1016/j.jmatprotec.2018.09.034
[22] R.H. Ding, Cast. Tech. **09**, 2122-2125 (2017). DOI: https://doi.org/10.16410/j.issn1000-8365.2017.09.017
[23] Z.J. Weng, K.X. Gu, K.K. Wang, Mater. Sci. Eng. A. **772**, 1-8 (2020). DOI: https://doi.org/10.1016/j.msea.2019.138698
[24] Z.Q. Tian, K.X. Wei, W Wei, Heat Treat. Met. **42** (02), 54-58 (2017). DOI: https://doi.org/10.13251/j.issn.0254-6051.201
[25] X.Y. Ji, F.W. Jin, Hot Process. Tech. **48** (16), 32-35 (2019). DOI: https://doi.org/10.14158/j.cnki.1001-3814.2019.16.006
[26] G.P. Tang, W.R. Huang, Heat Treat. Met. **41** (6), 36-45 (1998). DOI: https://doi.org/10.1088/0256-307X/16/12/013